ARTICLES

Combustion Synthesis as a Novel Method for Production of 1-D SiC Nanostructures

Andrzej Huczko,*,† Michał Bystrzejewski,† Hubert Lange,† Agnieszka Fabianowska,† Stanisław Cudziło,‡ Andrzej Panas,‡ and Mateusz Szala‡

Department of Chemistry, Warsaw University, Pasteur 1 Str., 02-093 Warsaw, Poland, and Department of Engineering, Chemistry and Technical Physics, Military University of Technology, 00-908 Warsaw, Poland

Received: February 17, 2005; In Final Form: April 21, 2005

1-D nanostructures of cubic phase silicon carbide (β-SiC) were efficiently produced by combustion synthesis of mixtures containing Si-containing compounds and halocarbons in a calorimetric bomb. The influence of the operating parameters on 1-D SiC formation yield was studied. The heat release, the heating rate, and the chamber pressure increase were monitored during the process. The composition and structural features of the products were characterized by elemental analysis, X-ray diffraction, differential thermal analysis/ thermogravimetric technique, Raman spectroscopy, scanning and transmission electron microscopy, and energy-dispersive X-ray spectrometry. This self-induced growth process can produce SiC nanofibers and nanotubes ca. 20−100 nm in diameter with the aspect ratio higher than 1000. Bulk scale Raman studies showed the product to be comprised of mostly cubic polytype of SiC and that finite size effects are present. We believe that the nucleation mechanism involving radical gaseous species is responsible for 1-D nanostructures growth. The present study has enlarged the family of nanofibers and nanotubes available and offers a possible, new general route to 1-D crystalline materials.

Introduction

The discovery of carbon nanotubes (CNTs)[1] has stimulated a great deal of interest in formation and characterization of other one-dimensional (1-D) nanostructures, including inorganic materials (metals, ceramic, glasses) and organic materials (biomolecules, polymers).[2] Such nanomaterials as nanotubes, nanowires, and nanorods have great potential for improving our understanding of the fundamental concepts of the roles of both dimensionality and size on physical properties, as well as for potential applications in nanoelectronics, optics and materials science.[3] Therefore, how to produce bulk 1-D nanostructures has to become one of the main targets of present nanoscience. As an example, many methods have been developed for CNTs growth under high-temperature conditions. This requirement can be also met by a fast exothermic decomposition of explosives which produces a huge amount of heat, and results in extreme conditions leading to the creation of unusual structures that are otherwise difficult to make.[4,5]

Many researchers have used the heat generated by exothermic reactions in the synthesis of nanomaterials.[6] This process employing redox compounds and mixtures (popularly known as combustion synthesis, self-propagating high-temperature synthesis SHS, or thermolysis) was shown to produce submicron SiC[7] and a host of other materials: oxides, borides, cermets, nitrides, and silicides.[8−10]

The combustion synthesis is based on the fact that the strong exothermic reaction can propagate rapidly through the solid reactants. The process begins with an activation period.[9,11,12] Once initiated, a self-sustaining reaction propagates through the powder mixture as a combustion process which is completed within a few seconds. The release of the reaction heat results in an abrupt increase of the temperature. During the course of reaction, rapid solidification may create structures that would be unstable under normal conditions, e.g., rapid cooling can lead to nucleation of 1-D nanocrystallites without any growth.[8,12] Because of the gas evolution, the products can be disintegrated during the process, forming very fine particulates of friable agglomerates.

Recently,[12] we reported that 1-D Si-containing nanometric structures with a high aspect ratio can be prepared through the defluorination of poly(tetrafluoroethylene) (PTFE) using the combustion synthesis route. Zhang et al.[13] mineralized PTFE by grinding with proper additives. Electrochemical defluorination of PTFE can lead to new nanostructures, e.g., carbyne-like or polyyne-containing carbon.[14−16] Highly mesoporous carbon and polymeric carbon were produced by combustion synthesis of mixtures containing PTFE and alkali metals.[17,18] The formation route of carbon nanotubes, through polyyne from PTFE was also performed.[15,19] Koch[20] calculated very high flame temperature of ∼5600 K upon ignition the mixtures of graphite fluoride and magnesium, resulting in the formation of low-ordered carbon.

The carbon, which is prepared by combustion dehalogenation of PTFE, is unstable and reactive and can be used not only as a precursor to form novel nanocarbons,[12] but also other interesting compounds, e.g., 1-D SiC nanocrystallites.[21] Silicon carbide as an outstanding large-gap semiconductor exhibits a set of unique physical parameters, which makes it a promising

* Corresponding author. E-mail: ahuczko@chem.uw.edu.pl.
† Warsaw University.
‡ Military University of Technology.

10.1021/jp050837m CCC: $30.25
Published on Web 08/10/2005

TABLE 1: Calorimetric, Elemental, and XRD Analyses[a]

reactant composition (wt %)	heat of reaction (kJ/kg)	C (wt %)	H (wt %)	phases identified
Si (26.0)/PTFE (74.0)	5650	79.6	0.2	SiC (s), Si (s), C (s)
FeSi (35.5)/PTFE (64.5)	5020	44.2		SiC (s), Si (m), C (m), Fe_3Si (m), Fe_5Si_3 (m)
$CaSi_2$ (57.8)/PTFE (42.2)	4900	8.3		SiC (s), Si (s), C (m), CaF_2 (s)
$CaSi_2$ (37.7)/$C_{12}F_{10}$ (62.3)	5030	44.5		SiC (s), Si (s), C (s), CaF_2 (s)
$CaSi_2$ (39.6)/C_2Cl_6 (60.4)	3100	17.2		SiC (s), Si (s), $FeSi_2$ (s)
$CaSi_2$ (16.8)/C_6Cl_6 (83.2)	2430	64.3	0.8	SiC (s), Si (s), $FeSi_2$ (s), C (w)
$CaSi_2$ (46.8)/C_6Cl_6 (53.2)	3020	15.4		SiC (s), Si (s), $FeSi_2$ (s)
$CaSi_2$ (43.2)/SPVC (56.8)	1970	22.6		SiC (s), Si (s), $FeSi_2$ (s)
$CaSi_2$ (30.2)/PTFE (49.8)/ $(C_5H_5)_2Fe$ (20.0)	4880	20.9	2.0	SiC (s), Si (w), FeSi (w), C (m), CaF_2 (s), Fe_5Si_3 (m)

[a] s-strong; m-medium; w-weak.

candidate for the fabrication of microelectromechanical systems (MEMS) and other high-temperature and harsh-environment applications while its high thermal conductivity is fundamental in terms of heat dissipation. In addition, SiC has a high Young's modulus and mechanical hardness, which makes it an attractive material to be used in composites.[22] Semiconductor SiC nanoparticles are expected to show luminescence by the quantum size effect.[23] If SiC were fabricated in the form of 1-D nanostructures, it would have new properties resulting from both its marked shape-specific and quantum-confinement effects. Due to its intensive blue-green emission, SiC nanowires may find an application in light-emitting diodes (LEDs) and also have great potential for use as electron emitters.[24]

Several methods of preparing 1-D SiC nanostructures have been reported.[24−29] However, all these methods are quite involved and require high temperature and long processing times. In this paper, we describe the spontaneous formation of 1-D SiC nanostructures by reductive dehalogenation of typical perhalogenated hydrocarbons (as precursors) with Si-containing compounds.

Experimental Section

Combustion synthesis was carried out in a closed stainless steel reactor of 1050 mL in volume. The starting two- and three-component mixtures were prepared in the form of a pellet made from fine powders (particle size below 100 μm) compressed at 10 MPa. The combustion process was initiated by an electrically heated reaction promoter attached to the top of the pellet. To evaluate the influence of environmental conditions, the chamber was filled with various gases at different initial pressure, or else the mass of the starting charge was changed. A series of combustion reactions were carried out to optimize the yield of a sought product. At least two runs were performed for each mixture. After the combustion was completed, the gaseous products were vented. The products, very voluminous spongelike gray solids, were collected for further examination.

A variety of measuring and analytical techniques were used to characterize the products. Heat effects accompanying the combustion process were measured with a water calorimeter.[21] According to the free energy calculations ($\Delta G°$), the sought reactions are thermodynamically spontaneous and the formation of solid carbon and carbides is possible. TG/DTA analyses were performed with a SETARAM Labsys TG-DTA/DSC apparatus.[12] The heating rates across the whole combustion wave were evaluated from the temperature measured within the pellet by using K type thermocouple.[12] The combustion reaction resulted with an abrupt pressure increase which was monitored by using quartz pressure transducers (PCB Piezotronics Inc., USA). By using the instruments presented elsewhere,[12] the elemental analysis, X-ray diffraction (XRD), Raman spectroscopy, scanning and transmission electron microscopy (SEM/TEM), and energy-dispersive X-ray spectroscopy (EDS) were employed to characterize the solid products.

TABLE 2: Operating Parameters of $CaSi_2$/PTFE Combustion Synthesis

initial mass of reactants (g)	combustion environment	initial pressure (MPa)	mass of collected spongelike product (g)
5	air	0.1	no product
10	air	0.1	2.0
15	air	0.1	4.4
20	air	0.1	9.8
25	air	0.1	8.1
30	air	0.1	7.5
20	air	below 0.1	10.1
20	air	0.3	3.4
20	argon	0.1	4.8
20	argon	0.3	4.0
20	argon	0.6	2.7
20	nitrogen	0.1	8.0
20	nitrogen	0.6	2.8
20	helium	0.1	7.1
20	oxygen	0.1	2.0
20	carbon dioxide	0.1	4.4

Results and Discussion

The combustion synthesis yielding 1-D SiC nanomaterial (according to EDX analyses) was carried out by using different Si-containing reductants (Si elemental, FeSi, $CaSi_2$) and organic oxidants-perhalogenated hydrocarbons precursors (PTFE, $C_{12}F_{10}$, C_2Cl_6, C_6Cl_6, SPVC) and, in one case, ferrocene $(C_5H_5)_2Fe$, added as a catalyst. The initial compositions, together with the results of calorimetric measurements, elemental and XRD analyses, are presented in Table 1.

It is worth mentioning here that C_6Cl_6 was used earlier as a source material in the synthesis of SiC nanowires.[30] However, the reaction (with $SiCl_4$ and metallic sodium as the reductant) was carried in the autoclave at 700 °C during 5−12 h. Other perhalogenated compounds react with $CaSi_2$ analogously to PTFE.[12]

A set of combustion synthesis was performed in which the operating parameters (starting mass of reactants, initial pressure and combustion environment) were altered. All other variables were kept constant. The experiments were carried out for $CaSi_2$/PTFE = 57.8/42.2 mixture as the following analyses (described below) had proven that it is the most favorable composition for 1-D SiC formation. For each run the following data were gathered: initial mass of pellet and pressure, and the mass of spongelike product collected after the combustion in the reactor. Table 2 shows the results of these parametric studies.

The results show that the yield of reaction, i.e., the $CaSi_2 \rightarrow$ 1-D SiC (the main component of the spongelike product, see

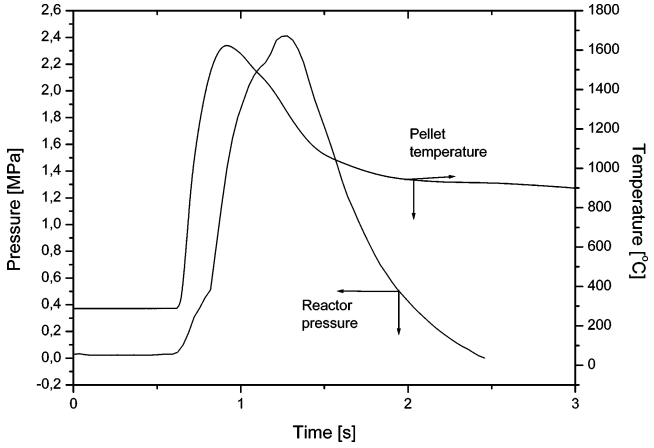

Figure 1. Temperature and pressure histories of $CaSi_2$/PTFE combustion synthesis.

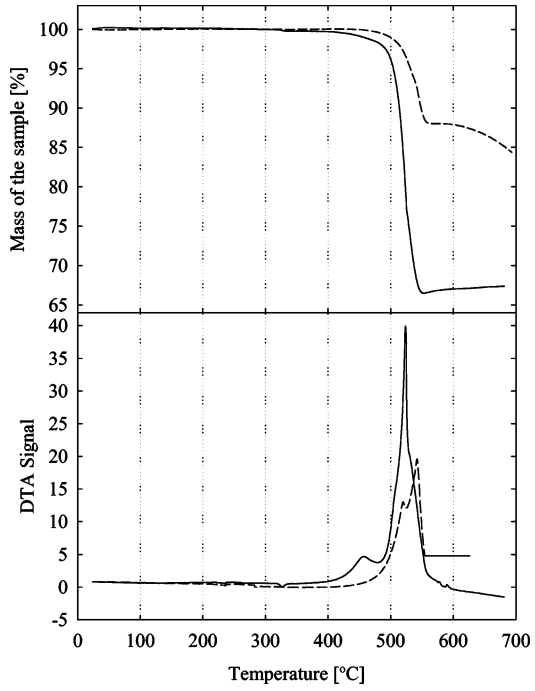

Figure 2. DTA/TG curves for the combustion synthesis of $CaSi_2$/PTFE (57.8/42.2) and $CaSi_2/CF_{0.8}$ (51.4/48.6) mixtures.

below) conversion, is strongly dependent on the combustion parameters. There is an optimal initial mass of reactants for the volume of the reactor used (ca. 20 g) and initial pressure (ca. 0.1 MPa), which yield the highest mass of the desired product and the highest conversion rate. It is very likely, however, that high yield of the SiC nanofibers could be also obtained while using the higher mass of reactants and increased reaction volume. The reaction atmosphere also strongly influences the process performance with the best results obtained in runs carried out in molecular gases (air, nitrogen), this probably due to their higher heat capacity and better quenching properties. In the case of pure oxygen, the direct high temperature partial oxidation of reactants cannot be ruled out. The morphology of the product does not depend heavily on the process environment. Only the nanofibers obtained under helium atmosphere are quite different comparing to other gases (see SEM/TEM images below). The results of these parametric studies indicate that the nucleation mechanism involving radical gaseous species is responsible for the product formation.

Calorimetric Measurements. The heat release accompanying the combustion was measured for different initial compositions

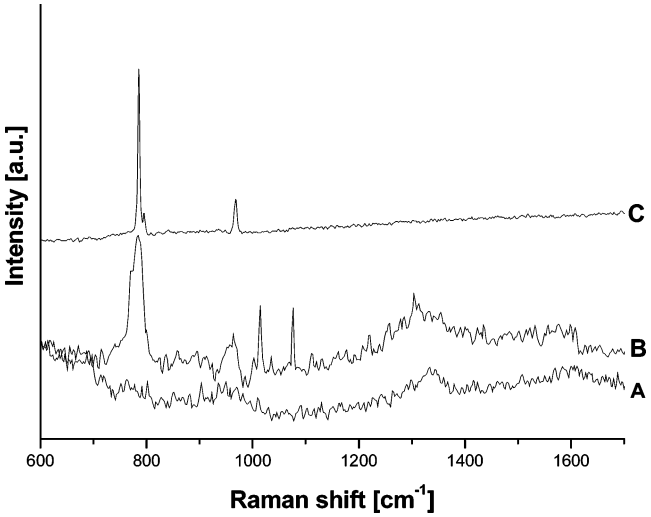

Figure 3. Raman spectra: (a) as-obtained product from $CaSi_2$/PTFE (57.8/42.2) sample; (b) same as in panel a, purified; (c) reference β-SiC.

and the average results of measurements are collected in Table 1. The heats of reactions range considerably—from ca. 2000 kJ/kg ($CaSi_2$/SPVC) to 5650 kJ/kg (Si/PTFE). They account for only ca. 70% of the theoretical exothermal effects calculated assuming the chemical equilibrium in the combustion wave.[30] Such significant changes of heat release for different reactants and their contents are accompanied by resulting varied combustion temperatures, so that the synthesis conditions inside the combustion wave change also dramatically. The general rule is that the heat of combustion for mixtures containing chlorinated hydrocarbons as oxidizing agents is lower by a half from that of containing fluorocarbons (Table 1).

Elemental and XRD Analyses. The oxidants have covalent C−F and C−Cl bonds that, when dissociated, will produce more reactive lower carbon−halogen (molecular and radical) species. Once the C−F(Cl) bonds are broken, carbon is forced to react either itself forming soot, or other compounds, e.g., carbides. Depending on the starting reactants, the carbon content of the solid products varied between 8 and 80 wt %. The higher content of carbon can be, obviously, related to the lower content of the other products (e.g., volatile metal fluoride), which, in the case of Si-containing mixtures, is gaseous SiF_4. Calcination of the product (see purification procedure below) resulted in a distinct decrease of free carbon content due to its oxidation. The residual carbon can be only related to carbide phases resistant against oxidation at the heating temperature. Phase identification of as-obtained products was carried out using the XRD patterns with different crystalline materials (silicon carbide, calcium fluoride, iron silicides, and unreacted silicon) identified. The intense peaks can be indexed to the β-SiC lattice structure with stacking faults.[31] The graphite-like phase (turbostratic graphite) was also found in the products with the strongest peak (002) at 2θ between 26.5° and 26.65°. The evolving fluorine reacted either with silicon (which escaped the reaction zone as SiF_4 gas) or with calcium (solid CaF_2 formation). Thus, the highest content of turbostratic graphite was found, as expected, in an Si/PTFE product. The combustion in Si/F systems resulted in much higher heat release and, consequently, higher temperatures comparing to Si/Cl compositions. Thus in the Si/F systems the elemental carbon condensed mostly as graphite microcrystallites while in the latter case amorphous carbon was formed. The iron silicide presence in the products can be related to the residual iron in the starting $CaSi_2$.

Temperature, Heating Rate, and Pressure Increase Measurements. The combustion synthesis is accompanied by the

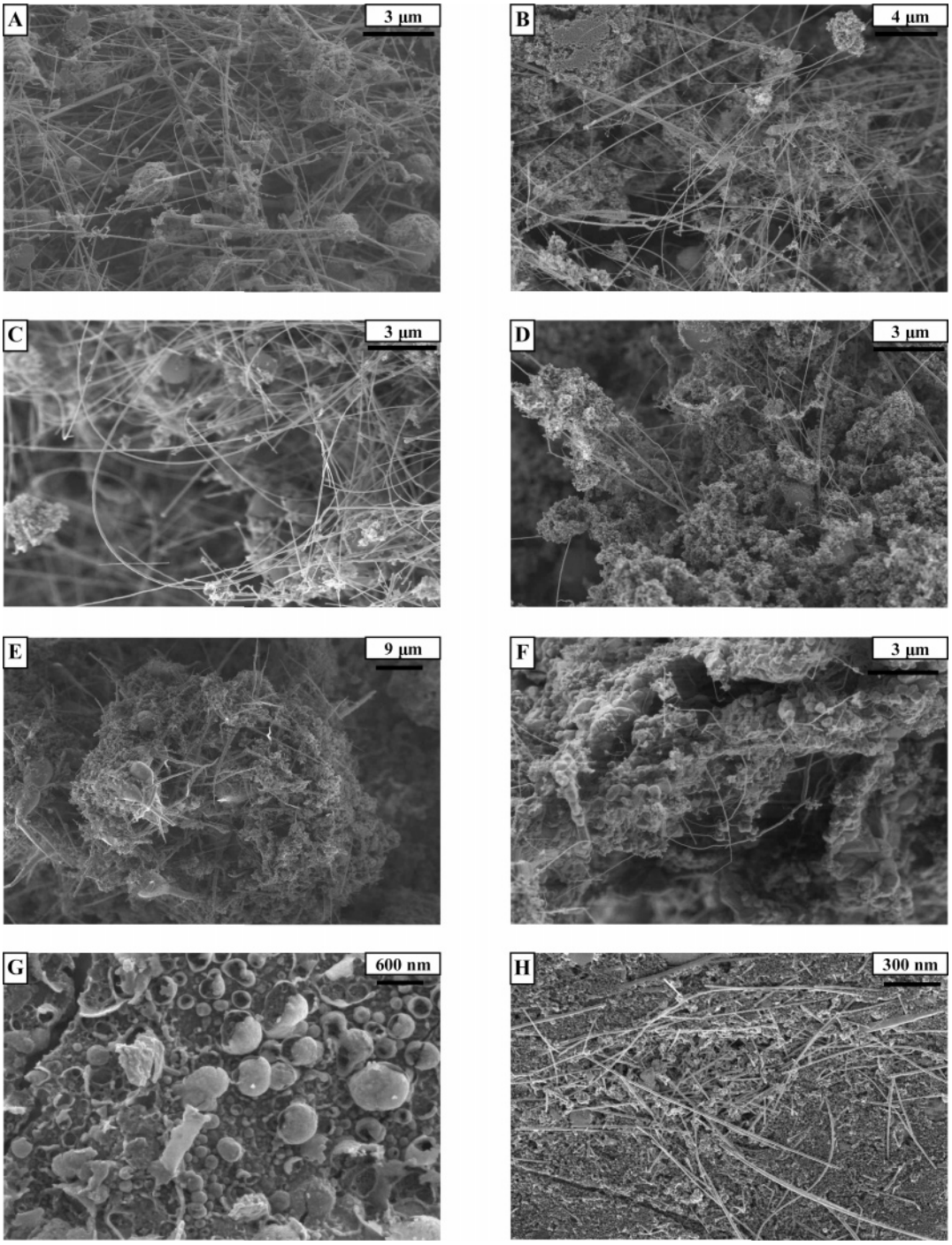

Figure 4. SEM images: (A) Si/PTFE (26.0/74.0) sample; (B) FeSi/PTFE (35.5/64.5) sample; (C) $CaSi_2$/PTFE (57.8/42.2) sample; (D) $CaSi_2$/$C_{12}F_{10}$ (37.7/62.3) sample; (E) $CaSi_2$/C_2Cl_6 (39.6/60.4) sample; (F) $CaSi_2$/C_6Cl_6 (46.5/53.5) sample; (G) $CaSi_2$/SPVC (43.2/56.8) sample; (H) $CaSi_2$/PTFE/$(C_5H_5)_2Fe$ (30.2/49.8/20.0) sample.

abrupt evolution of heat resulting in high temperature and pressure in the system. The latter one is additionally augmented by the generation of gaseous radical and molecular (SiF_4) species. The results of temperature and pressure measurements (for $CaSi_2$/PTFE combustion synthesis in air) are shown in Figure 1. Thus, the high heating rate and pressure increase equal to ca. 3.2×10^4 K s^{-1} and 7.9×10^6 Pa s^{-1}, respectively, were obtained.

DTA/TG Measurements. The chemical transformations during the combustion were followed by the DTA/TG measurements (Figure 2). In $CaSi_2$/PTFE and $CaSi_2$/$CF_{0.8}$ (for comparison) mixtures, exothermic processes commence at about 400 °C. This is also the temperature at which mass of the samples begins to decrease, so that the reactants evidently do not react in the condensed phase. The exothermic reactions with the gaseous products (mainly monomer, C_2F_4) of PTFE[32] and $CF_{0.8}$ decomposition are evidenced by the respective sharp exothermal effects on the DTA curve (at 523.8 and 542.4 °C, respectively) resulting from these reactions. The recorded weight losses show that, under the experiment conditions, only a part of the products of oxidant decomposition is fixed by the reductant ($CaSi_2$) in the form of condensed products—ca. 10% in the case of PTFE and ca. 37% for $CF_{0.8}$.

Raman Spectroscopy. Raman spectroscopy was used to determine the formation of β-SiC, α-SiC, and any residual Si and C in the specimen. Figure 3 shows typical spectra for the

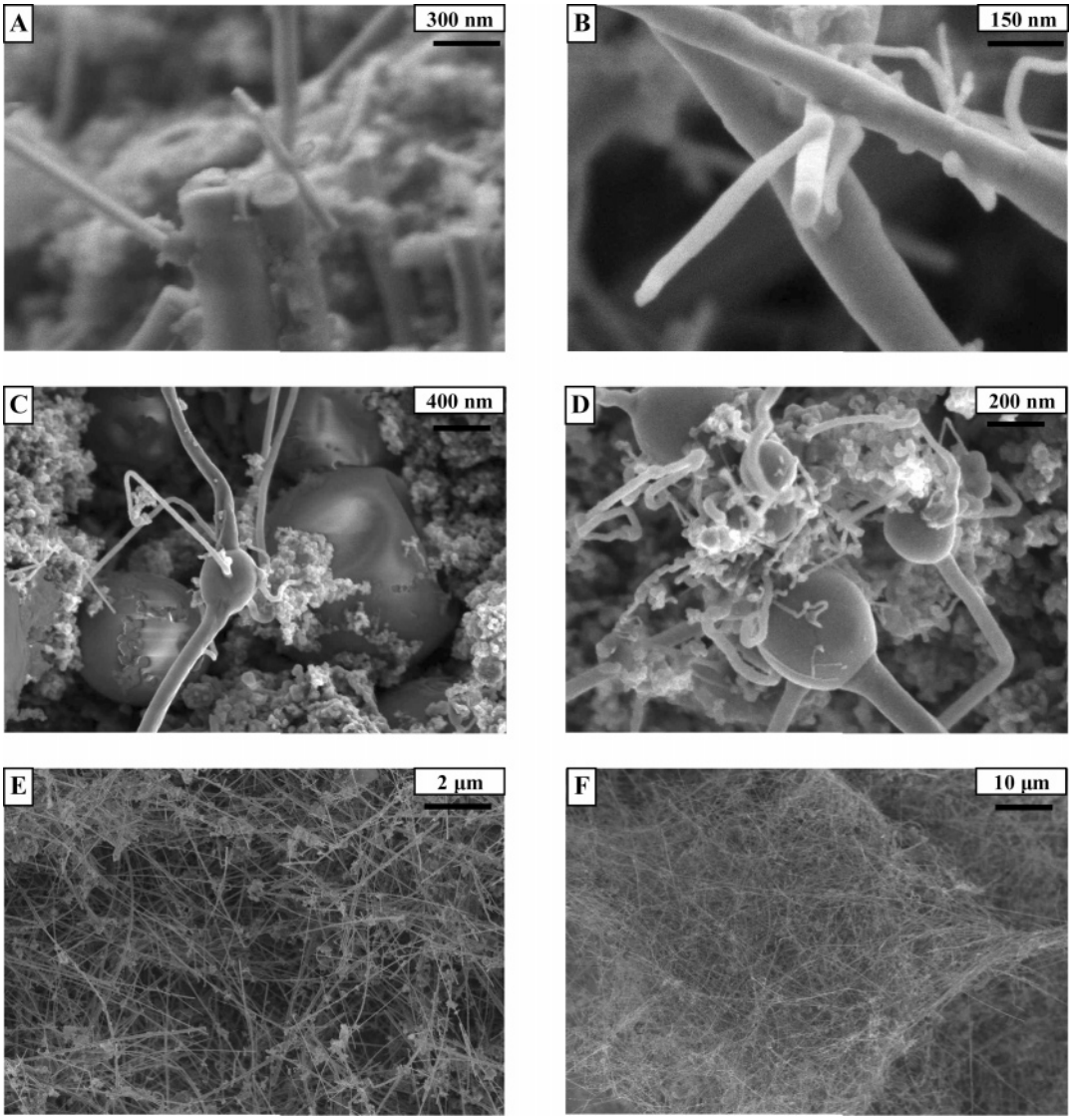

Figure 5. SEM images: (A and B) $CaSi_2$/PTFE (57.8/42.2) sample, in air; (C and D) $CaSi_2$/PTFE (57.8/42.2) sample, in helium; (E) Si/PTFE (26.0/74.0) sample, purified; (F) $CaSi_2$/PTFE (57.8/42.2) sample, purified.

as-obtained (a) and purified (b) product (for the purification procedure see below) and for a reference sample (c). The β-SiC is characterized by sharp peaks at 795 and 970 cm^{-1} arising from transverse optical (TO) and longitudinal optical (LO) phonos, respectively. The Raman spectral features of the purified product are strikingly different from the reference sample. The two lines, both with a broad tail (resulting from the existence of strong overlapping in this spectral range) are shifted toward lower energy. A mixture of different SiC polytypes (with dominating cubic form) along with disorder in the structure and stacking faults (shown in HRTEM image below) can explain this in agreement with the EDX studies. Finite size effects originated from the small grain sizes within the SiC nanofibers can also contribute to a broad tail toward low frequencies. There are also two broadened peaks corresponding to the characteristic D peak and G peak of graphite at 1330 and 1570 cm^{-1}, respectively. Currently further studies are in progress to elucidate the origin of two unidentified peaks (at around 1015 $cm^{-1}$and 1075 cm^{-1}) which cannot correspond to crystalline SiO_2 (825 cm^{-1}).

SEM and TEM. The morphology of combustion products is shown by SEM and TEM images (Figures 4−6). We detected various types of novel nanostructures. 1-D SiC nanostructures produced from present route typically have diameters ranging from $\sim$ 20 to several tens of nanometers and with lengths up to several tens of microns (Figures 4 and 5). They were present in almost all samples. However, for $CaSi_2$/PTFE starting mixture, the yield of nanofibers is significantly higher. The electron images revealed the presence of threadlike features, as if 1-D nanostructures were linked together in a spaghetti-like manner. The threadlike microstructures corresponded to varied diameters in a relatively wide range with the aspect ratio well above 10^3. A higher content of nanofibers was observed for fluorine-containing oxidants. Thus, a high-temperature resulting from the combustion of these compositions (Table 1) seems to be essential for their efficient growth.

Surprisingly, no nanofibers have been found in the product resulting from the combustion of $CaSi_2$/SPVC composition (Figure 4G). Instead, the high content of nanosized egg-shell-like structures (nanocarbon materials?) in this product was observed. The presence of hydrogen and chlorine in this starting oxidant, highly chlorinated PVC $(C_3H_5Cl)_n$, leads very likely here to the formation of gaseous HCl which may hamper the growth of fibers. Moreover, the heat of this combustion process was the lowest for this composition thus preventing the efficient evolution of gaseous intermediate reactants. Thus, despite the fact that the crystalline SiC was detected (XRD) in products, the temperature was probably too low to allow for the efficient

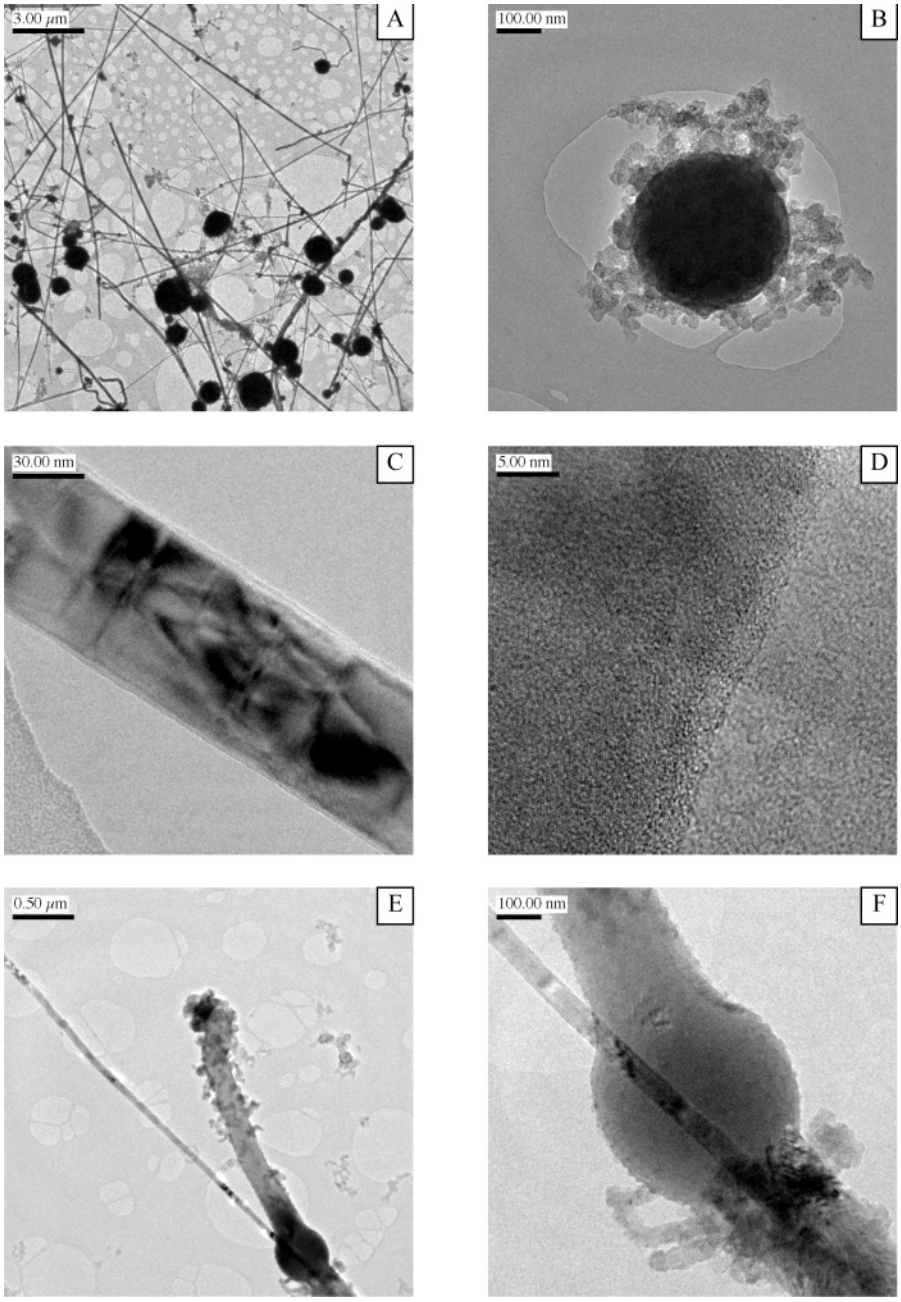

Figure 6. TEM/HRTEM images: (A−D) $CaSi_2$/PTFE (57.8/42.2) sample, in air; (E and F) $CaSi_2$/PTFE (57.8/42.2) sample, in helium.

transport of gaseous species and growth of SiC nanofibers. The fibers formed during the combustion of $CaSi_2$/PTFE)/$(C_5H_5)_2$-Fe composition (Figure 4H) display slightly different dimensions: shorter, straight and thicker. The study is under way to determine the composition of the nanostructures resulting from these latter runs.

SEM examinations also revealed that the part of SiC nanofibers can be open-ended tubes as Figure 5A,B would suggest. $CaSi_2$/PTFE combustion in helium (Figure 5C,D) surprisingly yielded flask-shaped nanostructures (nanoflasks). The nanoflask has an ovoid or a spherical bulbous base from which the nanofiber(s) grows, lengthening one-dimensionally. The fibers taper off slightly along their axes from thicker tips connected with bulbs. The approximate diameter distribution of the base of the nanoflasks was 100−300 nm, while the diameter of the elongated neck of the flasks was approximately 50−100 nm. The study is under way to both explain its formation (catalytic effect?) and better characterize the obtained nanostructures. These nanoflasks might be useful nanoelements due to their relatively large base, which makes it easy to manipulate them.

Elemental, XRD, Raman, and EDS analyses have shown that, along with SiC crystallites, the as-obtaind products of $CaSi_2$/PTFE combustion contain turbostratic graphite, calcium difluoride, silicon and silicon dioxide.[12] To obtain the pure SiC nanofibers, the combustion products were first calcinated in air at 700 °C for 2 h in order to remove the elemental carbon. After the calcinations, the silicon and silicon dioxide were removed by boiling the product suspension in KOH solution (30 wt %) under reflux for 8 h. The product was washed with plenty of water and exposed to boiling sulfuric acid (96 wt %) for 4 h. In this stage, calcium fluoride was transformed into calcium sulfate. Finally, to remove the latter compound, the sample was boiled in a hydrochloric acid (36 wt %) under reflux for 4 h. The final product was filtered, and the deposit was washed with plenty of water. Figures 5E and F show SEM images of the purified material for Si/PTFE and $CaSi_2$/PTFE compositions, respectively. The carbon content (elemental analysis) in the purified

product varied between 28.55 and 28.76 wt % (with hydrogen between 0.34 and 0.36 wt %, and nitrogen between 1.05 and 1.20 wt %). Thus, the chemical purity of the isolated 1-D SiC could be estimated to be at least 98.2 wt %.

TEM (Figure 6) showed that the resulting nanofibers have primarily smooth and straight whiskerlike morphology with some of them possessing bends and kinks, and appeared to be rigid, displaying dimensions similar to those observed by SEM. Figure 6A reveals the overview of the produced bulk sample, which consisted of SiC nanofibers and other products (Figure 6B), with very few carbon particles attached to the fibers surface walls (Figure 6E,F). HRTEM and EDX were performed in order to obtain information about the structure and composition of the products. Figure 6B demonstrates Ca- and F-containing (EDX analysis) product, evidently formed (spherical shape) from the liquid-phase solidification, covered by soot nanoparticles. For the fibers, there is a high density of stacking faults and striations on the image (Figures 6C−F). The spacing of the crystallographic planes measured from the HRTEM image (Figure 6D) is ca. 0.25 nm, which is consistent with the reported value (JCPDS card, No. 29-1129) to the (111) lattice planes of the crystalline SiC. The HRTEM images of the SiC nanofibers showed no evidence of axial screw dislocations, suggesting that these nanostructures were not grown by the screw dislocation mechanism.[33] Instead, the liquid globules found, e.g., on the tip of the nanofibers (Figures 5C,D and 6E,F) could suggest the VLS mechanism.[34] However, much more work remains to be done to fully confirm such growth of these nanofibers. The chemical composition analysis by EDX spectroscopy in both SEM and TEM confirmed that the atomic ratio of Si atoms to carbon atoms in the nanofibers was approximately the same as that of a reference SiC crystal. Further insight into the structure of the nanofibers shows (EDX) that the center nanofiber is wrapped in a uniform thin (ca. 3 nm) outer layer of SiO_2. It is apparent that these fibers, with their close-packed atomic planes, should possess high tensile strengths and Young's modulus.

The as-obtained combustion product also contained other types of particles: uniform carbon nanoparticles, ca. 20−30 nm in diameter, and additionally huge spherical particles (unreacted $CaSi_2$, Si, and CaF_2), 0.2−1.5 μm in diameter (Figures 6A and B).

On the basis of the above results, the formation mechanism of 1-D SiC nanostructures could be proposed as follows, although the exact formation mechanism is not completely understood. The growth of such a unique fiber is related to the highly energetic conditions generated by the combustion synthesis.

The initiation of the combustion results in the fast temperature increase and the pyrolysis of reactants is commenced. It should be underlined that, e.g., PTFE is thermodynamically unstable against reductive defluorination. Therefore, the apparent chemical stability of PTFE appears to be only a kinetic one, and PTFE should be carbonized even with mild reductants.[14] The pyrolysis yields low molecular weight gaseous fragments/radicals (see DTA/TG results) with a dominating proportion of the monomers. It is possible that these gaseous species formed in the combustion zone will be constructed when they move from the central zone toward the colder area (e.g., water-cooled inner reactor wall). They expand rapidly and coalescence processes commence, the course of which depends heavily e.g., on the partial pressure of condensing species and quench environment. Hence the distinct influence of process variables (initial mass of reactants, gas and pressure; Table 2) on reaction yield. The freshly formed carbon atoms assemble either into hexagonal carbon clusters (which may grow into soot particles) or form other compounds. During this rapid SiC nucleation phase, Si and C atoms pack along its close-packed plane. This stage may last for a very short time. Meanwhile, oxygen (which unavoidably exists in the reactor) may also react with Si to form thin SiO_2 amorphous layer, partly sheathing the SiC. As a result, this cover may hinder the stacking of further atomic planes on top of this nucleus, thus preventing an increase in fiber diameter. Further growth can only proceed continuously in the close-packed atomic direction, i.e., the fiber axis direction. Thus, the resulting SiC fibers are relatively thin, and exhibit a unique crystal plane-axis relationship. Thus, the SiC clusters are produced by the gas-phase reactions of $SiX_{n(g)}^{\bullet}$ and $CX_{m(g)}^{\bullet}$ radicals which can be represented by

$$MeSi_{(s)} + (CX_2)_{n(s)} \rightarrow SiX_{n(g)}^{\bullet} + CX_{m(g)}^{\bullet} \rightarrow SiC_{(s)} + C + MeX_{n(s)} + SiX_{4(g)}$$

The presence of iron (impurity contained in the starting $CaSi_2$) may also initiate the fiber growth controlled by catalytic mechanism.[35] Iron was continuously transported into the coalescence zone and tiny Fe−Si−C alloy droplets were formed. With the continuous absorption and dissolving of halogen-containing Si- and C-related radicals, the SiC was nucleated and precipitated upon quenching into nanofiber morphology from supersaturated liquid iron alloy. When the process is finished, the Fe−Si−C alloy droplets condensed into iron silicide phase (confirmed by XRD).

All products are in nanometer size. This can be again explained, as the condensing reactants did not have enough time to grow into larger 3-D microcrystals due to the inherent short duration of the combustion reaction and the fast quench during product expansion.

Conclusions

In conclusion, we succeeded in synthesizing β-SiC nanofibers and nanotubes via a spontaneous dehalogenation of different alkyl and aryl halides with Si-containing reductants. The combustion process can produce a huge amount of heat, and results in high temperatures. As a result, starting reactants decompose and radical gaseous species are formed, which expand from the heat wave zone. The expansion of reactive radicals give a way to following quenching and coalescence processes. The rearrangements of several different atoms within miliseconds yield new nanosized morphologies. The process was successfully applied to various solid mixtures, particularly to $CaSi_2$/PTFE system.

Advantages of the combustion synthesis method for easily realizing scale-up of 1-D SiC nanocrystallites production include that it is a simple, fast and unique one-pot process without the need for a catalyst or template, is low-cost, and has high yield, and the starting reactants are readily available. It appears, however, that much more work remains to be done to fully understand the growth mechanism of SiC nanofibers and nanotubes.

Acknowledgment. This work was supported by the Committee for Scientific Research (KBN) through the Department of Chemistry, Warsaw University, under Grant No. 3 T08D 012 28.

References and Notes

(1) Iijima, S. *Nature* **1991**, *354*, 56.
(2) Rao, C. N. R.; Deepak, F. L.; Gundiah, G.; Govindaraj, A. *Prog. Solid State Chem.* **2003**, *31*, 5.

(3) Lieber, C. M. *Solid State Commun.* **1998**, *107*, 607.
(4) Zhu, Z.; Su, D.; Lu, Y.; Schlögl, R.; Weinberg, G.; Lin, Z. *Adv. Mater*. **2004**, *16*, 443.
(5) Lu, Y.; Zhu, Z.; Liu, Z. *Carbon* **2004**, *42*, 361.
(6) Patil, K. C. *Bull. Mater. Sci.* **1993**, *16*, 533.
(7) Narayan, J.; Raghunathan, R.; Chowdhury, R.; Jagannadham, K. *J. Appl. Phys.* **1994**, *75*, 7252.
(8) Aruna, S. T.; Rajam, K. S. *Mater. Res. Bull.* **2004**, *39*, 157.
(9) Chen, Y.; Hwang, T.; Marsh, M.; Williams, J. S. *Metall. Mater. Trans. A* **1997**, *28A*, 1115.
(10) Merzhanov, A. G. In *Chemistry of Advanced Materials*; Rao, C. N. R., Ed.; Blackwell Scientific: Oxford, 1993; p 19.
(11) Takacs, L. *Prog. Mater. Sci.* **2002**, *47*, 355.
(12) Huczko, A.; Lange, H.; Chojecki, G.; Cudziło, S.; Zhu, Y. Q.; Kroto, H. W.; Walton, D. R. M. *J. Phys. Chem. B* **2003**, *107*, 2519.
(13) Zhang, Q.; Matsumoto, H.; Saito, F. *Chem. Lett.* **2001**, 148.
(14) Kavan, L. *Chem. Rev.* **1997**, *97*, 3061.
(15) Yasuda, A.; Kawase, N.; Matsui, T.; Shimidzu, T.; Yamaguchi, C.; Matsui, H. *React. Funct. Polym.* **1999**, *41*, 13.
(16) Yasuda, A.; Mizutani, W. *Thin Solid Films* **2003**, *438*−*439*, 313.
(17) Shiraishi, S.; Kurihara, H.; Tsubota, H.; Oya, A.; Soneda, Y.; Yamada, Y. *Electrochem. Solid-State Lett.* **2001**, *41*, A5.
(18) Tanaike, O.; Hatori, H.; Yamada, T.; Shiraishi, S.; Oya, A. *Carbon* **2003**, *41*, 1759.
(19) Nishino, H.; Nishida, R.; Matsui, T.; Kawase, N.; Hochida, I. *Carbon* **2003**, *41*, 2819.
(20) Koch, E.-C. *Z. Naturforsch.* **2001**, *56 b*, 512.
(21) Huczko, A.; Lange, H.; Chojecki, G.; Cudziło, S.; Zhu, Y. Q.; Walton, D. R. M.; Kroto, H. W.; Presz, A.; Diduszko, R. Proceedings of the XVIth International Winterschool on Electronic Properties of Novel Materials "Molecular Nanostructures" Kirchberg, Austria, March 2−9, 2002. In *Abstr. Book*; p 50.
(22) Dong, Y.; Molian, P. *Appl. Phys. A* **2003**, *77*, 839.
(23) Oku, T.; Hirata, T.; Motegi, N.; Hatakeyama, R.; Sato, N.; Mieno, T.; Sato, N. Y.; Mase, M.; Niwane, M.; Miyamoto, N. J. *Mater. Res.* **2000**, *15*, 2182.
(24) Chang, K.-W.; Wu, J.-J. *Appl. Phys. A* **2003**, *77*, 769.
(25) Dai, H.; Wong, E. W.; Lu, Y. Z.; Fan, S.; Lieber, C. M. *Nature* **1995**, *375*, 769.
(26) Feng, D. H.; Jia, T. Q.; Li, X. X.; Xu, Z. Z.; Chen, J.; Deng, S. Z.; Wu, Z. S.; Xu, N. S. *Solid State Commun.* **2003**, *128*, 295.
(27) Keller, N.; Pham-Huu, C.; Ehret, G.; Keller, V.; Ledoux, M. J. *Carbon* **2003**, *41*, 2131.
(28) Wong, K. W.; Zhou, X. T.; Au, F. C. K.; Lai, H. L.; Lee, C. S.; Lee, S. T. *Appl. Phys. Lett.* **1999**, *75*, 2918.
(29) Zhang, Y.; Wang, E.; He, R.; Chen, X.; Zhu, J. *Solid State Commun.* **2001**, *118*, 595.
(30) Cudziło, S.; Huczko, A.; Lange, H.; Panas, A.; Trzciñski, W. Proceedings of the 30th International Pyrotechnics Seminar, Saint Malo, France, June 23−27, 2003. In *EuroPyro 2003 Proceedings*; pp 547−554.
(31) Shen, G.; Chen, D.; Tang, K.; Qian, Y.; Zhang, S. *Chem. Phys. Lett*. **2003**, *375*, 177.
(32) Książczak, A.; Boniuk, H.; Cudziło, S. *J. Therm. Anal. Cal*. **2003**, *74*(2), 569.
(33) Sears, G. W. *Acta Metall*. **1953**, *1*, 457.
(34) Wagner, R. S.; Ellis, W. C. *Appl. Phys. Lett*. **1964**, *4*, 89.
(35) Li, Y.; Xie, S.; Zhou, W.; Ci, L.; Bando, Y. *Chem. Phys. Lett*. **2002**, *356*, 325.